Electronic Supplementary Material (ESI) for Materials Advances.
This journal is © The Royal Society of Chemistry 2023

Remarkably Enhanced Upconversion Luminescence in Na^+ Co-doped Spinel Nanoparticles for Photothermal Cancer Therapy and SPECT Imaging

Annu Balhara[1,2], Santosh K. Gupta,[1,2*] Nidhi Aggarwal,[3] Swapnil Srivastava,[3] Jiban Jyoti Panda,[3#] Sourav Patra,[1,4] Avik Chakraborty,[1,5] Sutapa Rakshit,[1,5] Rubel Chakravarty,[1,4]

[1]*Homi Bhabha National Institute, Anushaktinagar, Mumbai – 400094, India*
[2]*Radiochemistry Division, Bhabha Atomic Research Centre, Trombay, Mumbai-400085, India*
[3]*Institute of Nano Science and Technology, Mohali, Punjab, India*
[4]*Radiopharmaceuticals Division, Bhabha Atomic Research Centre, Trombay, Mumbai-400085, India*
[5]*Radiation Medicine Centre, Bhabha Atomic Research Centre, Parel, Mumbai-400012, India*

To whom correspondence should be addressed. Electronic mail: * *santoshg@barc.gov.in (SKG) / #jyoti@inst.ac.in (JJP)

1.0 Experimental

S1. Synthesis:

The Ho^{3+} doped $ZnAl_2O_4$ and $ZnAl_2O_4$:1%Ho^{3+}, 5%Yb^{3+}, x%Na^+ (x = 0 to 10 mol %) samples were prepared by using solid state method. The precursors, ZnO (99.995 %), Al_2O_3 (99.995 %), Ho_2O_3 (99.995 %), Yb_2O_3 (99.99 %) and Na_2CO_3 were weighed in stoichiometric amounts and mixed evenly by grinding using mortar and pestle. The samples were calcined at 900 ^oC for 15 h followed by grinding and annealing at 1200 ^oC for another 15 h. The final product obtained was well grinded for further characterization and analysis.

S2. Instrumentation:

The phase determination of doped and codoped $ZnAl_2O_4$ samples was carried out using X-ray diffraction (XRD). The XRD patterns of $ZnAl_2O_4$:Ho^{3+}, Yb^{3+}, Na^+ samples were recorded on a Proto-AXRD bench top powder diffraction system using the Cu Kα line (λ = 1.5406 Å), and the scanned 2θ range is 15-80° with a scan rate of 2°/min. Fourier Transform Infrared Spectroscopy (FTIR) was utilized for structural analysis of powder samples, and was performed in ATR mode using the Bruker Alpha FTIR spectrometer in the region of 400-1200 cm^{-1}. The information about the elemental composition was attained with the help of energy dispersive spectroscopy (EDS) analysis by using the Bruker Nano GmbHX Flash detector 410-M (Berlin, Germany). Morphological studies and particle size analysis were done using the field emission scanning electron microscopy (Make: Carl Zeiss, Model: GEMINISEM300). Particle size distribution histograms were obtained by performing the size

measurements using the ImageJ Software, on the FE-SEM images with 40K resolution. TEM images were recorded with JEOL, JEM-2100F and 200 kV electron source. Na analysis was carried out using laser induced breakdown spectroscopy (LIBS) system. A common laboratory used experimental set-up was used in the current LIBS study. Laser-induced plasma was generated with the second harmonic (532 nm) from a *Q*-switched Nd: YAG laser (Brilliant B, Quantel, France) focused through a plano-convex lens (focal length 10 cm). The sample was mounted on an XYZ -translation stage (Velmex, USA). A collimator (CC52, Andor, UK) was placed at an angle of 45^{o} with respect to the incoming laser direction for light collection. The plasma emission captured by the collimator was feed to 750 cm focal length Czerny–Turner spectrometer (Shamrock SR750, Andor) equipped with a 2400 lines per mm grating. The measured resolution of the system was 25 pm with the simultaneous spectral range of 7 nm. Intensifier charge coupled device (ICCD), (iStar DH334T-18F-03, Andor, UK) embedded with delay generator coupled with spectrometer was used for emission light detection. Acquisition time delay (t_d) and gate width (t_w) of ICCD was in synchronization with Q-switch of laser and is controlled by Solis 4.01 software. For the present study laser energy of 45 mJ, t_d of 2.5 µs and t_w of 50 µs was used. The PL measurements were performed on a FLS1000 fluorescence spectrometer (Edinburgh Instruments, U.K.) equipped with a 980 nm 5W laser, a source for acquiring the UC emission spectra (in C.W. mode) and PL decay plots (in pulse mode), and PMT as the detector.

The positron annihilation lifetime spectra were recorded on powder samples using Na-22 as positron source. The resolution of the lifetime spectrometer was 180 ps and the spectra were analysed using PALSFit software.[1]

S3. Computational Details:

All the DFT calculations using projector augmented wave (PAW) pseudo potentials have been carried out using Vienna ab initio simulation package (VASP).[2, 3] Perdew−Burke−Ernzerhof (PBE) functional within the framework of generalized gradient approximations (GGA) were used during structural optimization.[4, 5] The kinetic energy cut off for plane wave basis set has been chosen at 500 eV. Tolerance of 10^{-6} eV for self-consistent iteration energy convergence has been chosen for all the calculations. Brillouin zone integration has been carried out by using Monkhorst and Pack scheme with Γ-centered k-point mesh value of 4 × 6 × 6 for 102 atom cell.[6] The figure for crystal structure has been generated using the graphical software, VESTA.[7]

S4. ***Production of ^{166}Ho***

Holmium (^{166}Ho) was produced via (n, γ) route by irradiation of holmium oxide (Ho_2O_3, 100 % natural abundance in ^{165}Ho) powder in Dhruva reactor for 7 days at a thermal neutron flux of 1.2×10^{14} $n.cm^{-2}.\ s^{-1}$.

S5. Photothermal effect of $ZnAl_2O_4:Yb^{3+}$, Ho^{3+}, Na^+

To investigate the photothermal effect of our upconverting materials, 1mg/mL solution of $ZnAl_2O_4:Yb^{3+}$, Ho^{3+}, Na^+ was prepared in ddH_2O. The prepared solution was added to a 10 mm path length quartz cuvette and was irradiated with 980 nm NIR laser at an intensity of $1W/cm^2$. The rise in temperature was recorded by a thermometer at different time intervals.

S6. Cellular uptake studies performed in C6 cells

The internalization of $ZnAl_2O_4:Yb^{3+}$, Ho^{3+}, Na^+ was observed in C6 rat glioma cells. C6 rat glioma cells were cultured in a 24-well plate with a cell density of 50,000 cells/well in Dulbecco's modified Eagle's medium (DMEM) supplemented with 5% FBS kept at 37 °C humidified with 5% of CO_2 for 24 h. After 24h, cells were treated with 40 µg/mL dose of $ZnAl_2O_4:Yb^{3+}$, Ho^{3+}, Na^+ for 2, 4, 6, and 8 h under 37 °C and 5% CO_2. After incubation, the cells were washed with 1x PBS thrice and were imaged under 10x using Carl Zeiss LSM 880 Confocal Microscope.

S7. In vitro biocompatibility study of the NPs performed in fibroblast cells

For exploring the biocompatibility of our upconverting material, standard 3-(4,5-dimethylthiazol-2- yl)-2,5-diphenyl tetrazolium bromide (MTT) assay was performed in L929 fibroblast cells. Briefly, L929 cells were cultured in a 96-well plate with a cell density of 10000 cells/well in complete DMEM media at standard conditions of 37 °C humidified with 5% of CO_2 for 24 h. After 24 h of incubation, the plate was treated with $ZnAl_2O_4:Yb^{3+}$, Ho^{3+}, Na^+ at varying concentrations. As the control group, the blank was added with pure culture. After an incubation of 24 h, 20 µL of MTT solution (5mg/mL) was added to each well, and all the wells were incubated at 37 °C for another 4 h. Then, the MTT containing media was discarded and 100 µL of DMSO was added to each well for 30 mins to dissolve the formazan. Finally, the absorbance of each well was measured by using a Tecan Multimode Microplate reader at 570 nm.

S8. In vitro anti-cancer efficacy of the NPs determined in C6 glioma cells

In vitro efficacy of $ZnAl_2O_4:Yb^{3+}$, Ho^{3+}, Na^+ was investigated in C6 cells by evaluating the percentage cell viability using MTT assay. Briefly, C6 cells were seeded in two different 96 well plates with density of 10,000 cells/well and were incubated for 24 h in a humified incubator maintained at 37 °C with 5% CO_2. Subsequently, both the plates were treated with different concentrations of $ZnAl_2O_4:Yb^{3+}$, Ho^{3+}, Na^+ (20 µg/mL, 40 µg/mL, 80 µg/mL, and 100 µg/mL) and further incubated for next 6 to 8 h for particles to be taken up by the cells. After incubation, each well in one plate was irradiated under 980 nm laser for 5 min at an intensity of 1W/cm^2. Further the cells were incubated till 24h, and the percentage cell viability was calculated via standard MTT assay kit.

S9. Scratch wound healing assay

C6 cells were seeded in two 24-well plate at a density of 50,000 cells/well. After full confluency, cells were incubated with varying concentrations of $ZnAl_2O_4:Yb^{3+}$, Ho^{3+}, Na^+ (20 µg/mL, 40 µg/mL, and 60 µg/mL). After 6 h, the cells were washed for thrice with 1x PBS and a scratch was made in each well in both the plates with a sterile plastic 200 µL micropipette tip. After wounding, the cells were washed for thrice with PBS, and fresh medium was added. 980 nm NIR-laser was irradiated to each well in one plate at an intensity of 1 W/cm^2 for 5 min and other plate was kept constant in a humified incubator maintained at 37 °C with 5% CO_2. The irradiated and non-irradiated cells were next imaged at 0h and 24h following laser exposure to analyse cellular migration into the scratch wounds by using a brightfield microscope.

S10. Synthesis of intrinsically radiolabeled $ZnAl_2O_4:Yb^{3+}$, $^{166}Ho^{3+}$, Na^+

The $ZnAl_2O_4$ nanophosphor could be radiolabeled with ^{166}Ho with near-quantitative yield by simply grinding $^{166}Ho_2O_3$ with inactive *$ZnAl_2O_4:Yb^{3+}$, Ho^{3+}, Na^+* formulation in a mortar pestle at room temperature for 15 minutes.

S11. Preclinical studies with intrinsically radiolabeled $ZnAl_2O_4:Yb^{3+}$, $^{166}Ho^{3+}$, Na^+

In order to determine the radionuclidic purity of the synthesized radionano formulation, the γ-ray spectrum of a small aliquot was recorded in HPGe detector coupled with multichannel analyzer (MCA). The radiochemical purity of $ZnAl_2O_4:Yb^{3+}$, $^{166}Ho^{3+}$, Na^+ was determined by size exclusion chromatography using PD-10 (Merck) column.[8] This was also corroborated by

radio-thin layer chromatography (radio-TLC) study in which 5 µL of radiolabeled agent was applied at 1.5 cm from bottom of a chromatographic plate (10 cm × 1 cm). The chromatogram was developed in 0.1 M citrate buffer. Subsequently, the plate was dried, cut into 1 cm pieces and counted in NaI (Tl) counter. The radiochemical purity of $ZnAl_2O_4$:Yb^{3+}, $^{166}Ho^{3+}$, Na^+ was determined by comparing the amount of activity that remained at the point of application (R_f = 0-0.1) to the amount of activity that migrated to the solvent front (R_f = 0.8-1.0).

The radiochemical stability of the nanoformulation was determined under physiological conditions at 37 °C. A small amount (~ 1 mg) of intrinsically radiolabeled $ZnAl_2O_4$:Yb^{3+}, $^{166}Ho^{3+}$, Na^+ was dispersed in 0.1 mL of deionized water by sonication. To the above suspension, 1.9 mL of phosphate buffered saline (PBS) or mouse serum was added and incubated at 37 °C. At different time intervals, the radiochemical purity of the radiolabeled nanoformulation was determined using size exclusion chromatography.

In vivo stability of intrinsically radiolabeled $ZnAl_2O_4$:Yb^{3+}, $^{166}Ho^{3+}$, Na^+ were confirmed by SPECT (Single Photon Emission Computed Tomography) scan with a CT (Computed Tomography) imaging study in healthy Wistar rats, weighting 150−220 g. The experiment in animals was performed with full compliance with the guidelines from the Institutional Animal Ethics Committee of Bhabha Atomic Research Centre. A suspension solution of $ZnAl_2O_4$:Yb^{3+}, $^{166}Ho^{3+}$, Na^+ were prepared in PBS and the rats were administrated with an aliquot of 0.1 mL (15-20 MBq) injected through the tail vein. The rats were anesthetized by inhalation of isoflurane and put in supine position in a SPECT scanner (GE Discovery NM/CT 670, US). Whole body scans were performed at different time intervals post-injection of the radiolabeled agent.

2.0 Discussion

2.1 Computational calculations for defect formation energy

In the present study, the doped systems have been constructed using 102 atoms supercell. Here, we have chosen only Zn lattice site for introducing the dopant element as observed in the experiment. The defect formation energies for doped systems have been computed using the relationship below.[9, 10]

$$E_{formation} = E_{defect} - E_{perfect} + q\sum n_x \mu_x \quad (1)$$

where, E_{defect} and $E_{perfect}$ are the energies of the doped and perfect $ZnAl_2O_4$, calculated with same cell size, respectively. μ_x indicates the chemical potential of the element X and n_x is

the number of element introduced (q = -1) or removed (q = +1) to produce the doped system. The calculated defect formation energies for the doping of different dopant element into $ZnAl_2O_4$ are provided in ***Table S1***.

Table S1: Calculated defect formation energy of doped $ZnAl_2O_4$ systems

System	Defect Formation Energy (eV)
Ho-doped $ZnAl_2O_4$	-1.20
(Ho, Yb, Na)-doped $ZnAl_2O_4$	-5.51

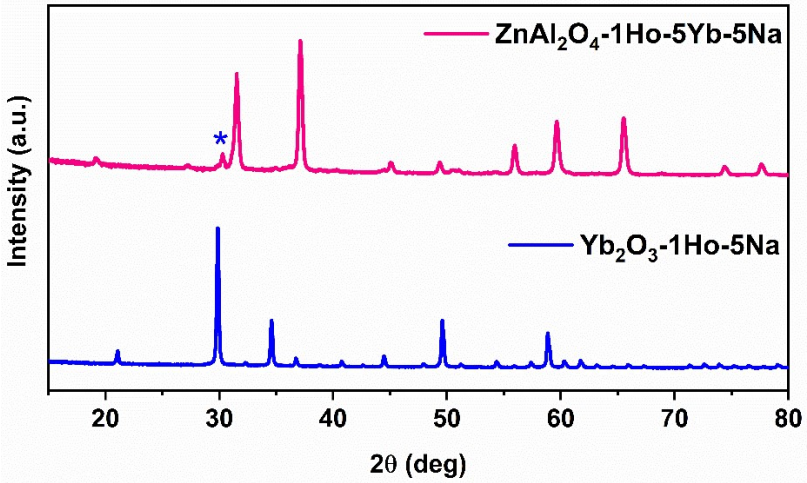

Figure S1: XRD patterns of Yb_2O_3:1%Ho^{3+}, 5%Na^+ and $ZnAl_2O_4$:1%Ho^{3+},5%Yb^{3+}, 5%Na^+ sample.

2.2 SEM Analysis

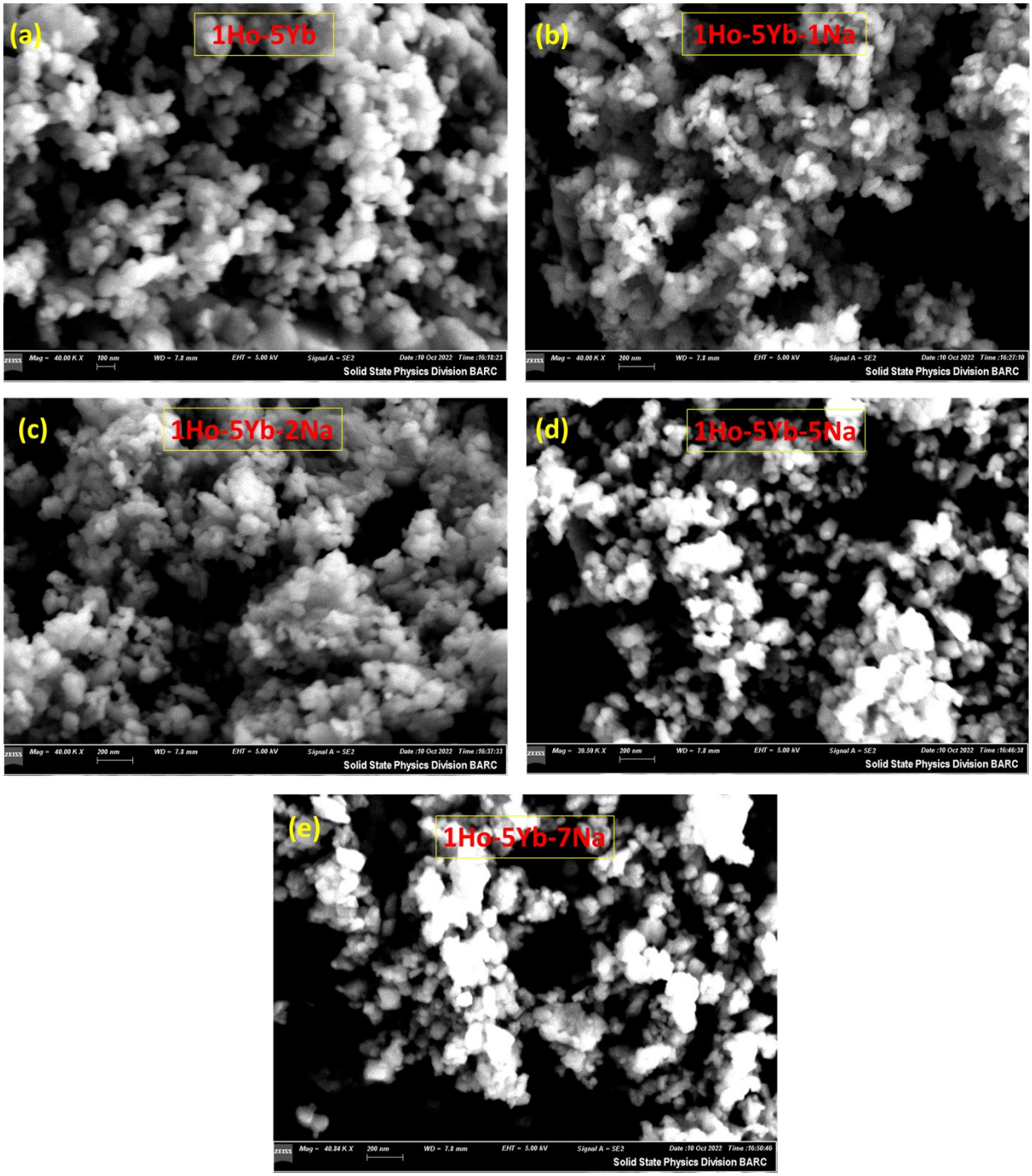

Figure S2: FE-SEM images of co-doped (a) $ZnAl_2O_4$:1%Ho^{3+}, 5%Yb^{3+}, and (b) $ZnAl_2O_4$:1%Ho^{3+}, 5%Yb^{3+}, 1%Na^{+}, (c) $ZnAl_2O_4$:1%Ho^{3+}, 5%Yb^{3+}, 2%Na^{+}, (d) $ZnAl_2O_4$:1%Ho^{3+}, 5%Yb^{3+}, 5%Na^{+}, and (e) $ZnAl_2O_4$:1%Ho^{3+}, 5%Yb^{3+}, 7%Na^{+} samples, [(a) Scale – 100 nm, Magnification:40.00 K ×, WD = 7.8 mm, EHT = 5.00 kV, (b-e) Scale – 200 nm, Magnification:40.00 K ×, WD = 7.8 mm, EHT = 5.00 kV].

2.3 EDS Analysis

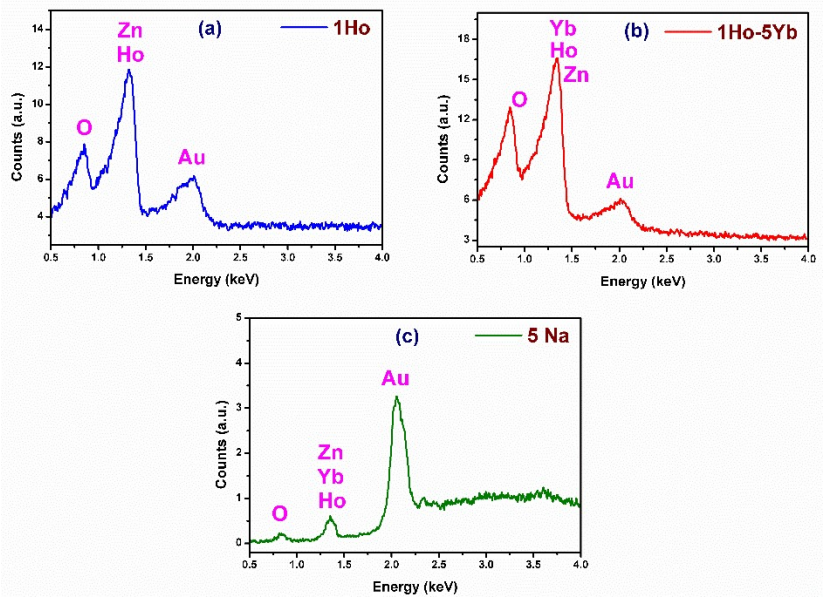

Figure S3: EDS spectra of (a) doped $ZnAl_2O_4$:1%Ho^{3+}, (b) codoped $ZnAl_2O_4$:1%Ho^{3+}, 5%Yb^{3+}, and (c) codoped $ZnAl_2O_4$:1%Ho^{3+}, 5%Yb^{3+}, 5%Na^{+} samples.

2.4 Sodium Analysis: Laser Induced Breakdown Spectroscopy (LIBS)

The LIBS emission spectra were acquired at an acquisition time delay of 2.5 µs. The increasing doping concentration in the crystal lattice can also be observed by plotting the emission line intensity against the doping concentration (***Figure S3a and b***). For both the emission lines, a linear increase in intensity with doping concentration was observed until 7% doping. At a higher doping, i.e., with 10% Na^{+} doping decrease in the emission intensity was seen due to the self-saturation effect, which is a well-documented phenomena in LIBS spectra for high concentration elements.

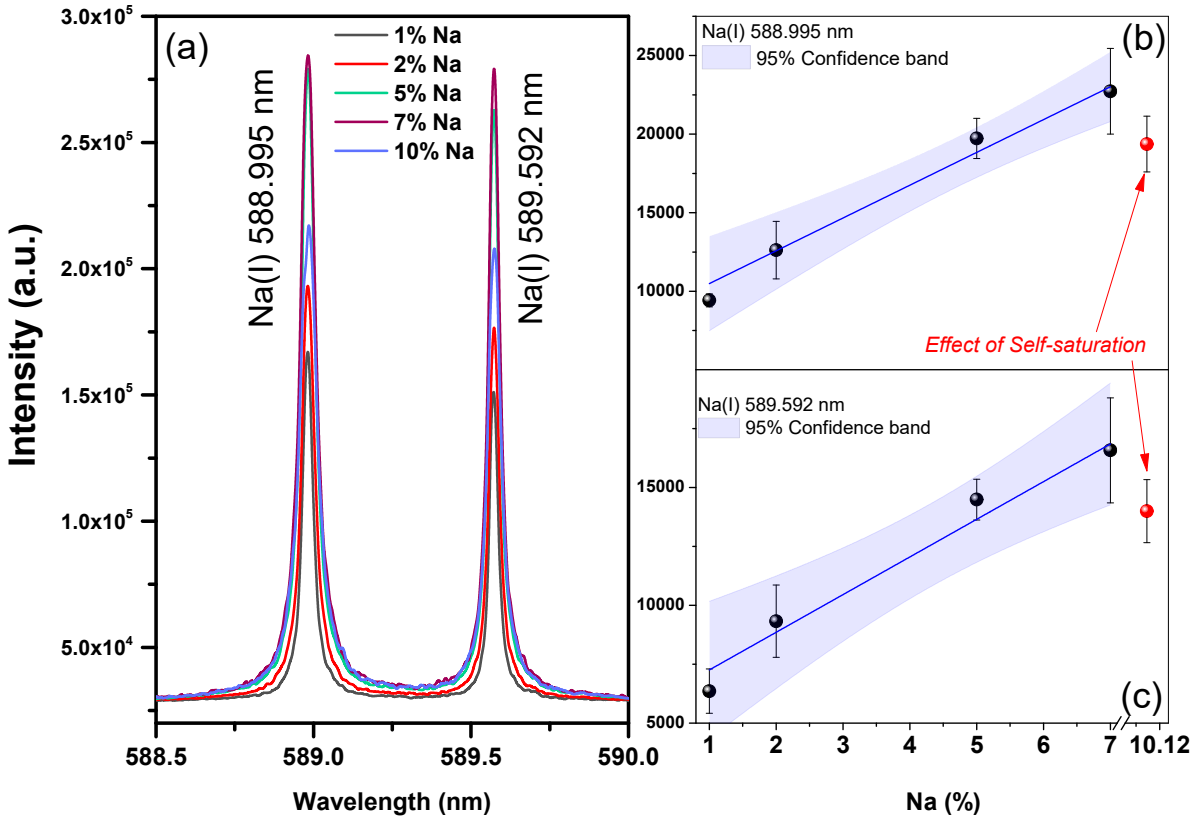

Figure S4: (a) LIBS emission spectra of codoped $ZnAl_2O_4$:1%Ho^{3+}, 5%Yb^{3+}, *x*%Na^+ (*x* = 1, 2, 5, 7 and 10 mol%) samples at acquisition time delay of 2.5 µs. (b and c) Linear increase of Na atomic emission line intensity with increasing Na^+ doping concentration. At 10% doping self-saturation of emission intensity for both the emission lines can be observed.

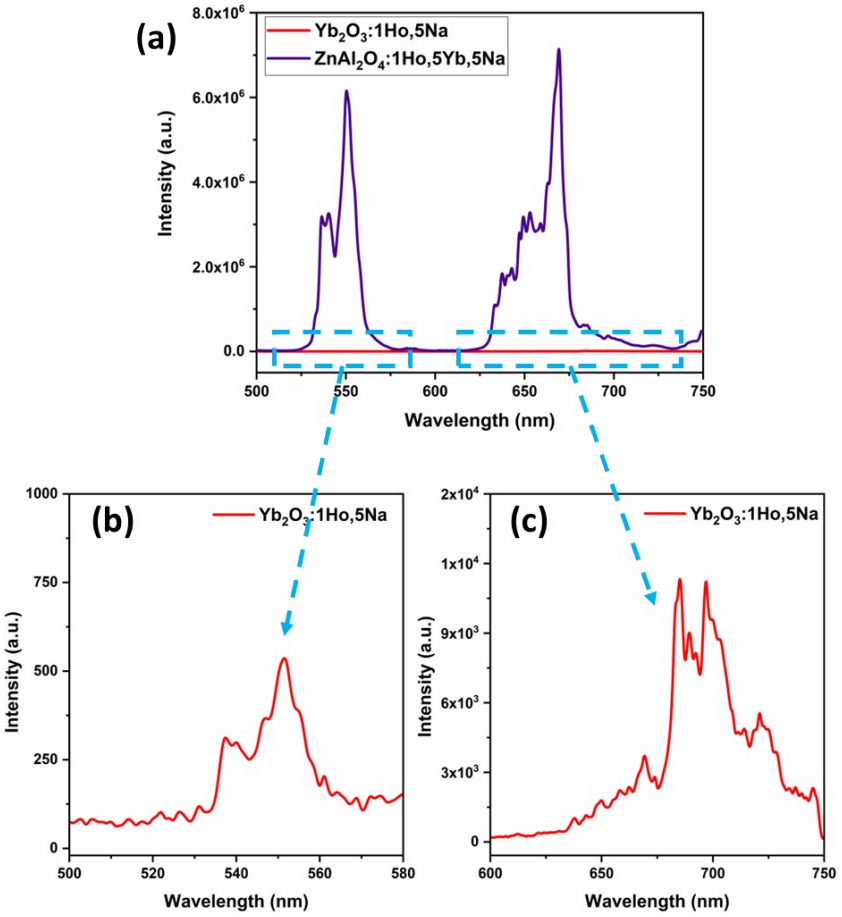

Figure S5: (a) Upconversion emission spectra of Yb_2O_3:1%Ho^{3+}, 5%Na^+ and $ZnAl_2O_4$:1%Ho^{3+},5%Yb^{3+}, 5%Na^+ sample under 980 nm excitation, (b and c) Zoomed in emission spectra of Yb_2O_3:1%Ho^{3+}, 5%Na^+ sample.

Table S2: Some of the recent reports wherein non-fluorescent metal ion is used as crystal field modulator to enhance UC emission in Ho^{3+}-Yb^{3+} co-doped phosphors

System	Enhancement in UC Emissions	Remarks	Ref.
$Y_2Ti_2O_7$:1Ho^{3+}/3Yb^{3+}/Zn^{2+} phosphor	Enhanced by ~92 times on Zn^{2+} doping compared to $Y_2Ti_2O_7$:1Ho^{3+}/3Yb^{3+} phosphor	Only green emission at 549 nm reported	11
YVO_4:Ho^{3+}-Yb^{3+}-K^+	Two-fold increase compared to YVO_4:Ho^{3+}-Yb^{3+} phosphor	green and red up-conversion emission on 980 nm excitation	12
Ho^{3+}/Yb^{3+}/Bi^{3+} co-doped $ZnGa_2O_4$ phosphor	Enhances up to 128 through co-doping of Yb^{3+} and 228 times via	Up-conversion of NIR light to visible light on 980 nm	13

	codoping of Yb^{3+}/Bi^{3+} ions	excitation	
$Ho^{3+}/Yb^{3+}/Li^{+}$ co-doped $ZnGa_2O_4$ phosphor	Enhanced up to 372 times via Yb^{3+} and 966 times via Li^{+} doping	UC emissions in visible and NIR reported on 980 nm excitation	[14]
$Ho^{3+}/Yb^{3+}/Mg^{2+}$ co-doped $CaZrO_3$	Four times on Mg^{2+} doping compared to $CaZrO_3$:Ho^{3+}/Yb^{3+} phosphor	Very weak UV blue, green, red and NIR emissions on excitation at 976 nm	[15]
$Ho^{3+}/Yb^{3+}/Li^{+}$ codoped Gd_2O_3 phosphor	Approx. 3 times on Li^{+} doping	green, red and NIR emissions on excitation at 976 nm	[16]
Gd_2WO_6:$Ho^{3+}/Yb^{3+}/Li^{+}$	Less than 3-fold on Li^{+} doping	green, red and NIR emissions on excitation with 976 nm	[17]
$ZnAl_2O_4$:$Ho^{3+}/Yb^{3+}/Na^{+}$ phosphor	Green emission enhanced up to 4×10^3 times via Yb^{3+} and 3.5×10^4 times via Na^{+} codoping Red emission enhanced up to 6.9×10^3 times via Yb^{3+} and 3.2×10^4 times via Yb^{3+}/Na^{+} codoping.	In addition to visible UC, we got very intense UVC UC as well which got further enhanced by ~7 times on sodium doping. This work shows demonstration of $ZnAl_2O_4$:$Ho^{3+}/Yb^{3+}/Na^{+}$ phosphor for theranostic and anti-cancerous applications.	***This work***

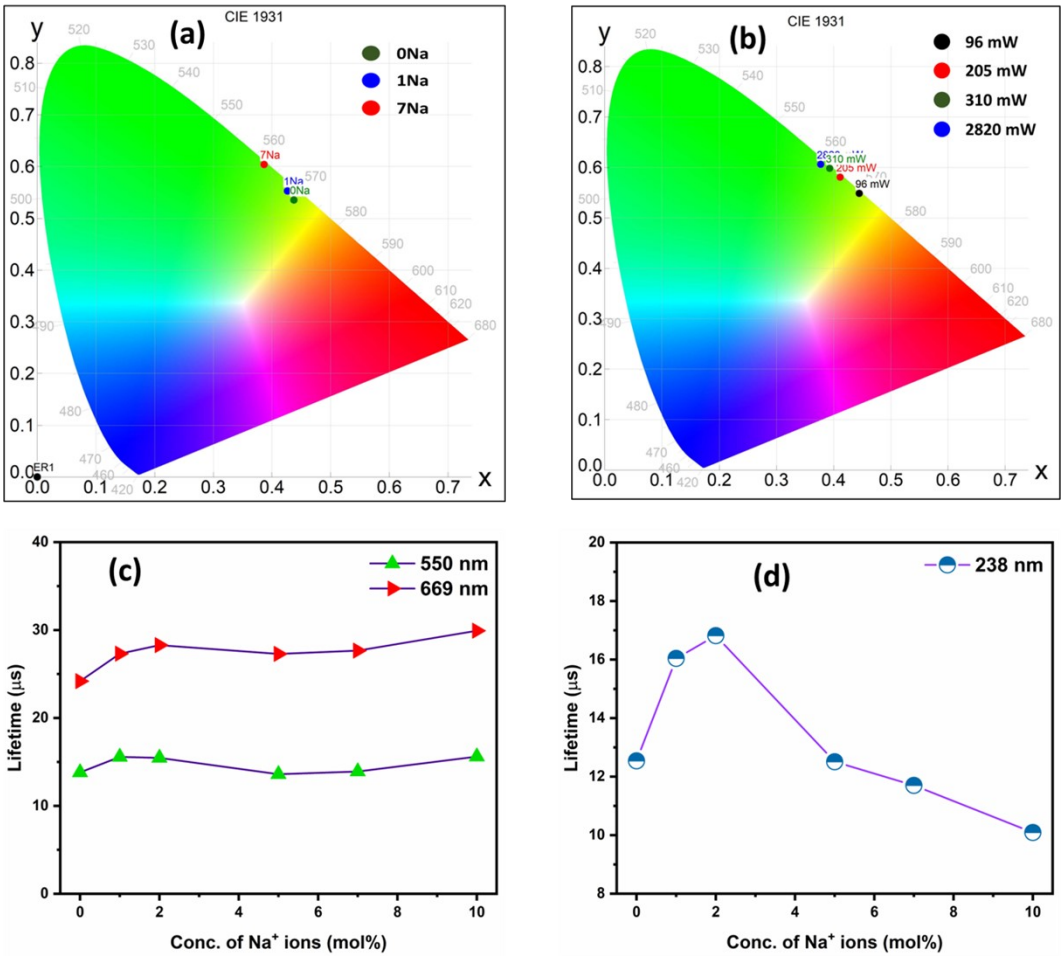

Figure S6: (a) CIE diagram of $Ho^{3+}/Yb^{3+}/xNa^{+}$ (x = 0, 1 and 7 mol%) co-doped $ZnAl_2O_4$ phosphors, and (b) CIE diagram of $ZnAl_2O_4$:$Ho^{3+}/Yb^{3+}/5Na^{+}$ phosphor at different laser excitation powers, and Variation of lifetime values with different codoping concentrations of Na^{+} ions for UC emissions at (c) 550 and 669 nm and (d) UV-C UC emission at 238 nm.

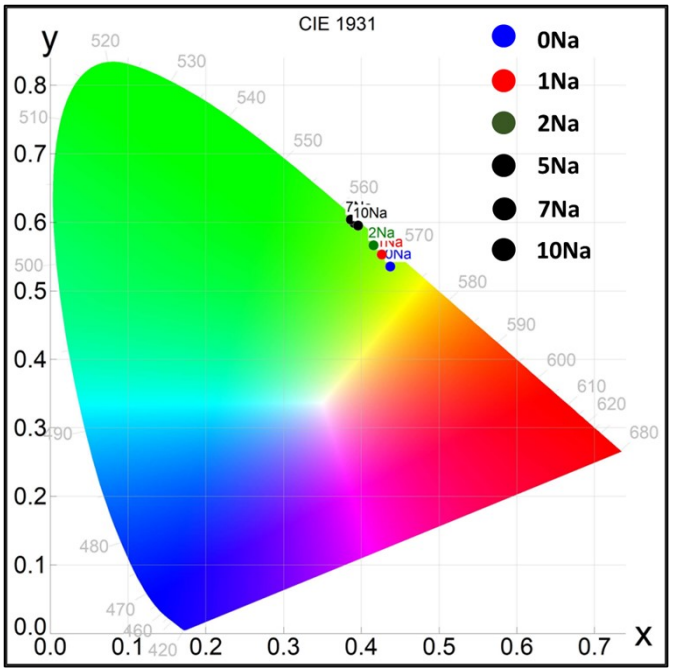

Figure S7: CIE diagram of $Ho^{3+}/Yb^{3+}/xNa^{+}$ (x = 0, 1, 2, 5, 7 and 10 mol%) co-doped $ZnAl_2O_4$ phosphors

2.5 *Color purity and CCT Analyses:*

The CIE diagram for different codoping concentrations of Na^{+} ion in the codoped $ZnAl_2O_4:Ho^{3+}/Yb^{3+}/xNa^{+}$ (x = 0, 1, and 7 mol %) under 980 nm excitations at 0.310 W is shown in ***Figure S6a***. CIE diagram for all codoping concentrations of Na^{+} ions is given in ***Figure S7***. The color of visible UC emission is tuned from yellowish-green in codoped $ZnAl_2O_4:Ho^{3+}/Yb^{3+}$ sample to green through codoping of Na^{+} ions.

The color purity analyses were performed to check the performance of the $ZnAl_2O_4:Ho^{3+}/Yb^{3+}/Na^{+}$ phosphor material by using the following relation:

$$\frac{\sqrt{\quad}}{\sqrt{\quad}} \qquad (2)$$

where (x_s, y_s), (x_i, y_i) and (x_d, y_d) represents the CIE coordinates of phosphor, the standard light source and dominant wavelength, respectively.[13] ***Table S3*** reveals the CIE coordinates, color purity and CCT values for $ZnAl_2O_4:Ho^{3+}/Yb^{3+}/xNa^{+}$ (x = 0, 1, 2, 5, 7, and 10 mol %) phosphors. ***Figure S6b*** represents the CIE diagram of $ZnAl_2O_4:Ho^{3+}/Yb^{3+}/5Na^{+}$ phosphor at different laser excitation powers (96, 205, 310 and 2820 mW). ***Table S4*** shows the CIE coordinates, color purity and CCT values for $ZnAl_2O_4:Ho^{3+}/Yb^{3+}/5Na^{+}$ phosphor at different laser excitation powers. In addition to the variation in sodium ions concentrations, the

emission can be tuned from CIE coordinates values of (0.445, 0.548) to (0.377, 0.606), by changing the laser power. The color purity values lie in the range of 95.6 to 98.5%.

The correlated color temperature (CCT) is an important parameter to get the insight about the cool and warm nature of emitted light. The CCT values have been evaluated by using CIE coordinates of the $ZnAl_2O_4:Ho^{3+}/Yb^{3+}/Na^+$ phosphors in the McCamy's formula[13] as below:

(3)

Where, $n = (x_s - 0.3320)/(0.1858 - y_s)$ and (x_s, y_s) denote the calculated values of CIE coordinates for the phosphors.

The CCT values changes from 3762 K to 4531 K with different codoping concentrations of Na^+ ions, and variation in the nature of emitted light was attained from cool to warm light. In addition, different CCT values were obtained for $ZnAl_2O_4:Ho^{3+}/Yb^{3+}/5Na^+$ at different laser excitation powers. The CCT values change from 3717 K to 4817 K on increasing the laser power, and the nature of green emission approach towards cool light range.

Table S3: CIE Coordinates, Color purity and CCT values for $ZnAl_2O_4:Ho^{3+}/Yb^{3+}/xNa^+$ (x = 0, 1, 2, 5, 7, and 10 mol %) phosphors.

Sample	(x_s, y_s)	Color Purity (%)	CCT (K)
0Na	(0.438, 0.535)	92.4	3762 K
1Na	(0.427, 0.553)	94.4	3981 K
2Na	(0.416, 0.566)	95.2	4173 K
5Na	(0.391, 0.599)	97.6	4604 K
7Na	(0.387, 0.604)	97.8	4680 K
10Na	(0.396, 0.595)	98.0	4531 K

Table S4: CIE Coordinates, Color purity and CCT values for $ZnAl_2O_4:Ho^{3+}/Yb^{3+}/5Na^+$ phosphor at different laser excitation powers.

Laser Power	(x_s, y_s)	Color Purity (%)	CCT (K)
96 mW	(0.445, 0.548)	98.5	3717 K
205 mW	(0.412, 0.581)	98.6	4277 K
310 mW	(0.393, 0.598)	98.2	4576 K
2820 mW	(0.377, 0.606)	95.6	4817 K

2.6 *Lifetime Measurements*

The decay dynamics of the $ZnAl_2O_4$:1%Ho^{3+}, 5%Yb^{3+}, *x*%Na^+ (*x*= 0, 1, 2, 5, 7 and 10 mol%) codoped samples at 550 and 669 nm UC emissions, were studied under 980 nm laser excitation using 0.310 W power. The curve fitting was performed using the monoexponential fitting for both 550 and 669 nm using the following relation:[18]

$$I(t) = I_0 + Ae^{\frac{-t}{\tau}} \quad (2)$$

Where, A denote the coefficients, and *I(t)* represent the emission intensity at time t and I_0 is the background or zero-offset. The terms 'τ' denote the luminescence lifetimes and are evaluated for the $^5F_4$/ $^5S_2$ and $^5F_5$ excited levels of Ho^{3+} ions for green and red UC emissions. An increment in the lifetime values of 550 and 669 nm was observed with the increase in the codoping concentration from 0 to 2 mol% of Na^+ ions (***Figure S6c***). The increase in the lifetime value till 2 mol% of Na^+ ions correlate well with the trend observed in the UC emission intensity for both, red and green emission. However, a decrement in the lifetime values was observed for 5 mol% of Na^+ ions, and increased again with higher codoping concentrations. ***Table S5*** summarizes the lifetime values obtained for different UC emissions under the 980 nm excitation.

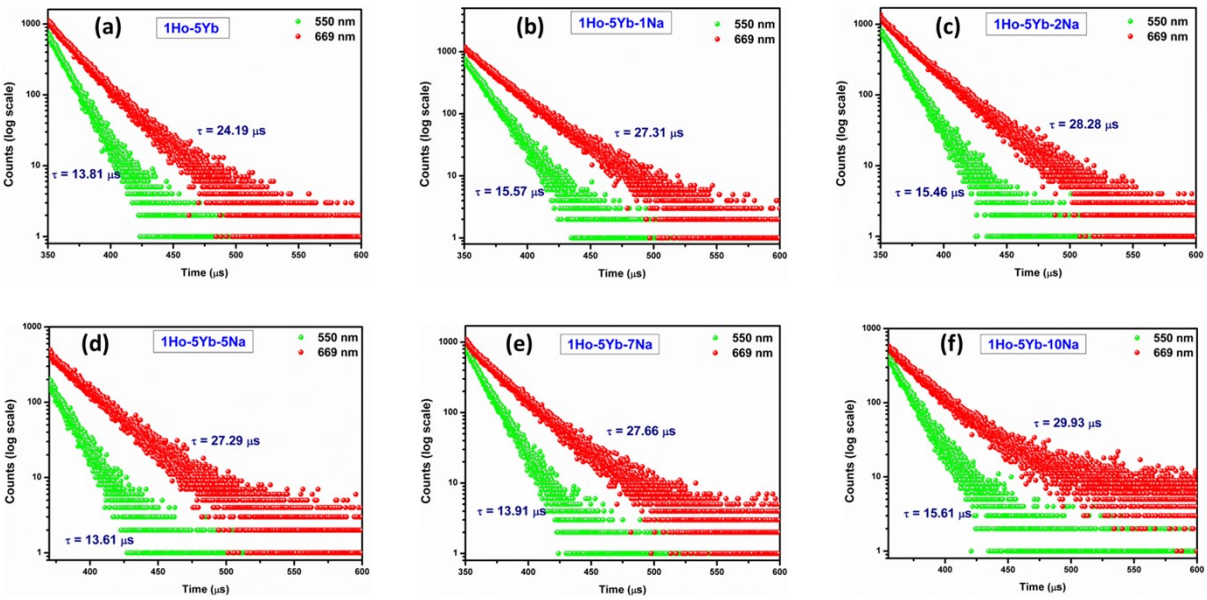

Figure S8: Lifetime decay plots of codoped $ZnAl_2O_4$:1%Ho^{3+}, 5%Yb^{3+}, *x*%Na^+ (*x* = 0, 1, 2, 5, 7 and 10 mol%) samples at 550 and 669 nm UC emissions.

Table S5: Lifetime values of codoped $ZnAl_2O_4$:1%Ho^{3+}, 5%Yb^{3+},*x*%Na^+ (*x* = 0, 1, 2, 5, 7 and 10 mol%) samples at 550, 669 and 238 nm UC emissions.

Sample	τ (550 nm) (μs)	τ (669 nm) (μs)	τ (238 nm) (μs)
1Ho-5Yb-0Na	13.81	24.19	12.54
1Ho-5Yb-1Na	15.57	27.31	16.04
1Ho-5Yb-2Na	15.46	28.28	16.82
1Ho-5Yb-5Na	13.61	27.29	12.51
1Ho-5Yb-7Na	13.91	27.66	11.70
1Ho-5Yb-10Na	15.61	29.93	10.09

The curve fitting of decay curves at 238 nm was performed using the expression in equation (2). The lifetime values increase up to codoping of 2 mol% of Na^+ ions, and then decreases on increasing the codoping concentrations of sodium ions (***Figure S6d***). The initial increase in the lifetime values can be attributed to the reduction of defect centers on Na^+ ions codoping.[19] However, the decreasing lifetime values at higher concentrations argue the back energy transfer (BET) from Ho^{3+} to Yb^{3+} and boost in the non-radiative processes.[20] Also, the particle size and crystallinity play a major role in the decay processes of UCL.

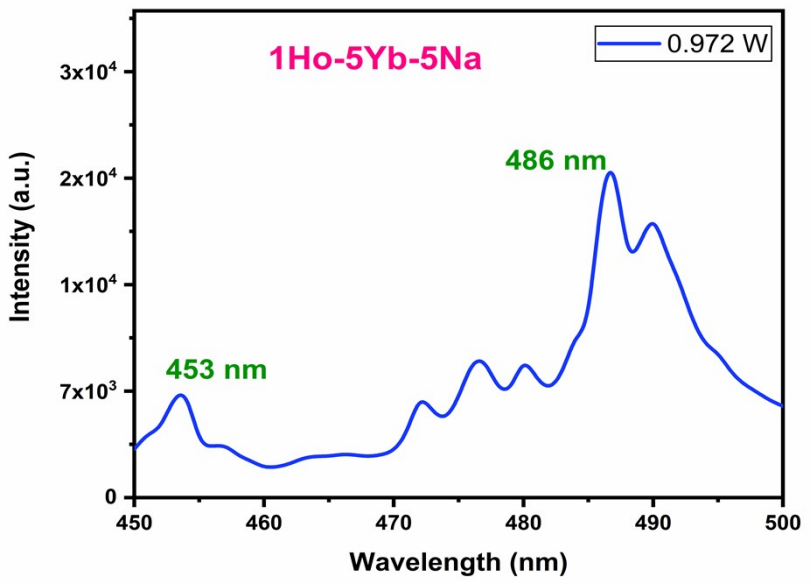

Figure S9: Zoomed in UC emission spectra of codoped $ZnAl_2O_4$:1%Ho^{3+}, 5%Yb^{3+}, 5%Na^+ sample from 450-500 nm, under a 980 nm laser excitation at a laser power of 0.982 W.

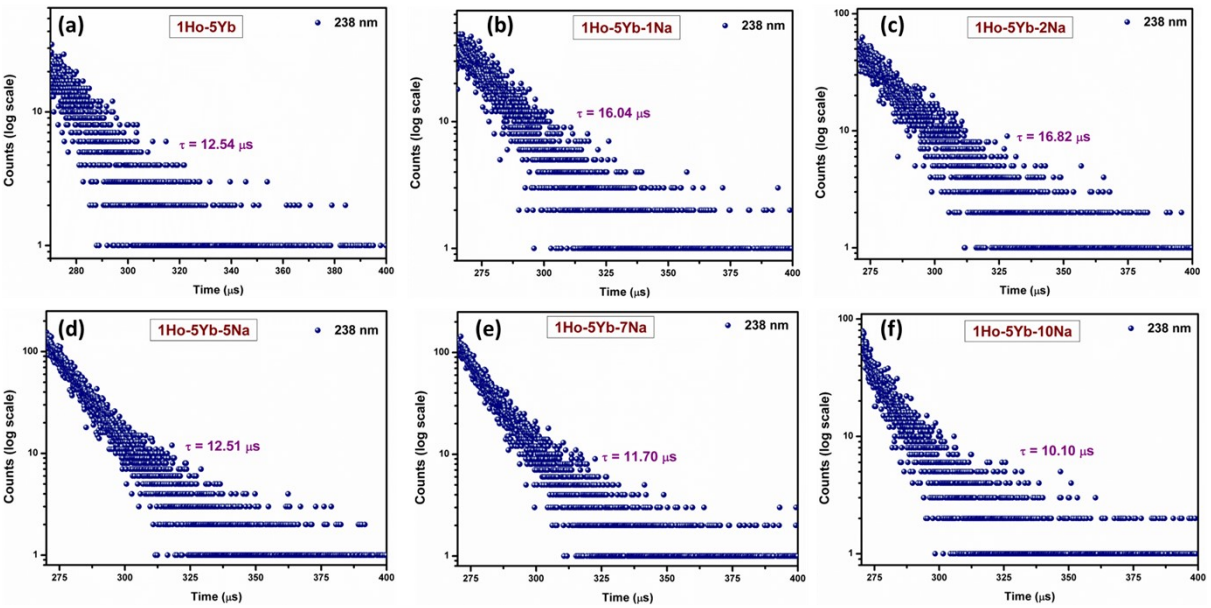

Figure S10: Lifetime decay plots of codoped $ZnAl_2O_4$:1%Ho^{3+}, 5%Yb^{3+}, *x*%Na^{+} (*x* = 0, 1, 2, 5, 7 and 10 mol%) samples at 238 nm UV-C UC emission.

2.7 *Positron annihilation Lifetime Spectroscopy (PALS):*

Positron annihilation lifetime spectra could be fitted well as sum of three lifetimes and were named as τ_1, τ_2 and τ_3 in increasing order of magnitude and the corresponding intensity of positrons annihilating with the respective lifetimes as I_1, I_2 and I_3. The longest lifetime (τ_3) was in the range of 1-1.5 ns and with intensity of 1-2% in all the cases and is expected due to positronium formation on the surface of the particles in the powder samples. The data corresponding to only 1%Ho doped $ZnAl_2O_4$ is given in the figure on the negative side of x-axis (-0.5%) for comparison. The average positron lifetime calculated from these two lifetime components is also given in the ***Figure S11***. The first lifetime component in oxides in the range of 150-170 ps is associated with positron annihilations in bulk with possible contributions from shallow positron traps like oxygen vacancies. The second positron lifetime in the range of 320-350 ps is expected due to large vacancy clusters like cation vacancies and their complexes with oxygen vacancies etc. with possible contribution from surface defects. It is seen from the figure that the positron lifetime in 1%Ho doped sample is lower than 1%Ho+5%Yb doped sample showing the creation of more vacancies with codoping of 5%Yb. The Ho^{3+}, Yb^{3+} are closer in size to Zn^{2+} and are much larger than Al^{3+}. The size similarity of the dopants with Zn^{2+} makes it the likely substitution site. The charge balance can be achieved either by antisite defects or cation vacancies. The observation of two lifetime

components or absence of saturation trapping in the defects suggests that both should be present.

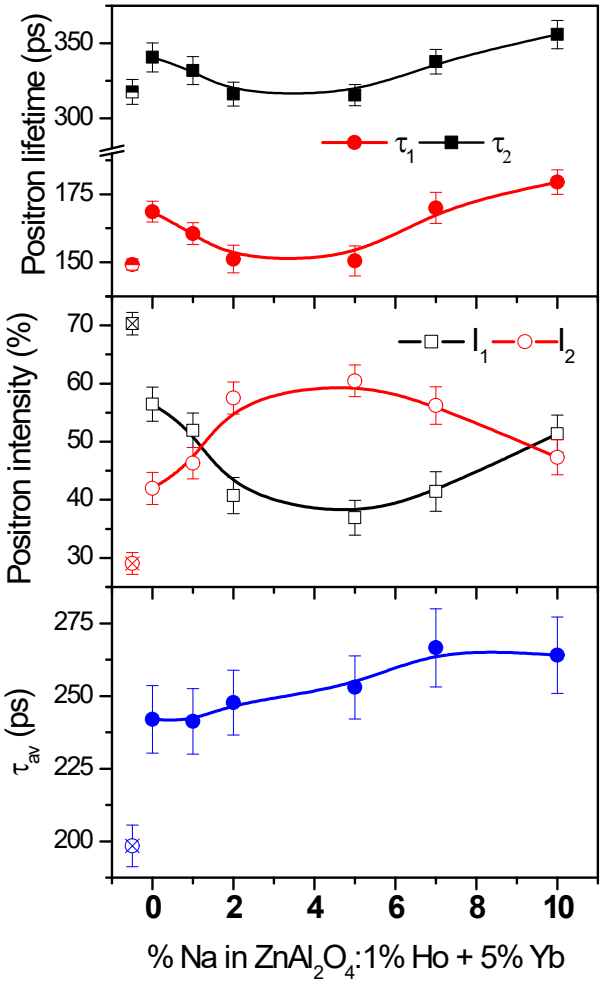

Figure S11: Positron lifetimes and intensities in Na^{+} doped $ZnAl_2O_4$:1%Ho, 5%Yb.

2.8. Role of Ho, Yb, and Na

To investigate the role of the dopant element on the enhancement of optical properties of $ZnAl_2O_4$. As can be seen from the ***Figure S12a*** and ***b***, the Fermi level shifts to the CB region in the presence of Ho. This is due to the fact the doping with Ho (usually at Ho^{3+}) at the Zn lattice site (usually at Zn^{2+}) make the system electron excess. Ho introduced discrete impurity states in the midgap position as well as adjacent to the CB. Thus, the effective band gap reduced to 1.62 eV and 2.15 eV. It can be noted that, both the discrete impurity states and CBM shows prominent presence of Ho f states, which (f-f transition) is responsible for the observed emission behaviour of Ho-doped $ZnAl_2O_4$. Interestingly, for the (Ho, Yb, Na)-doped $ZnAl_2O_4$ system, fully occupied impurity states, composed of Yb f state, appear close

to the CB (***Figure S12c***). More interestingly, Yb f impurity states appeared almost in the similar energy region of that of Ho f impurity states. Thus, Yb can act as a sensitizer for the Ho-doped $ZnAl_2O_4$ system. This is responsible for the observed enhancement of optical behavior for the tri-doped system. It can be noted that Na being an alkali metal ion does not contribute directly to the optical property by introducing impurity states. However, it plays a crucial role in compensating the charge mismatch arises due to doping with Ho and Yb. Thus, presence of Na reduces spontaneous formation charge compensating vacancy defects, which are well known source for charge carrier trapping centers. Thereby, the intensity of the emitting light increases significantly in the presence of Na.

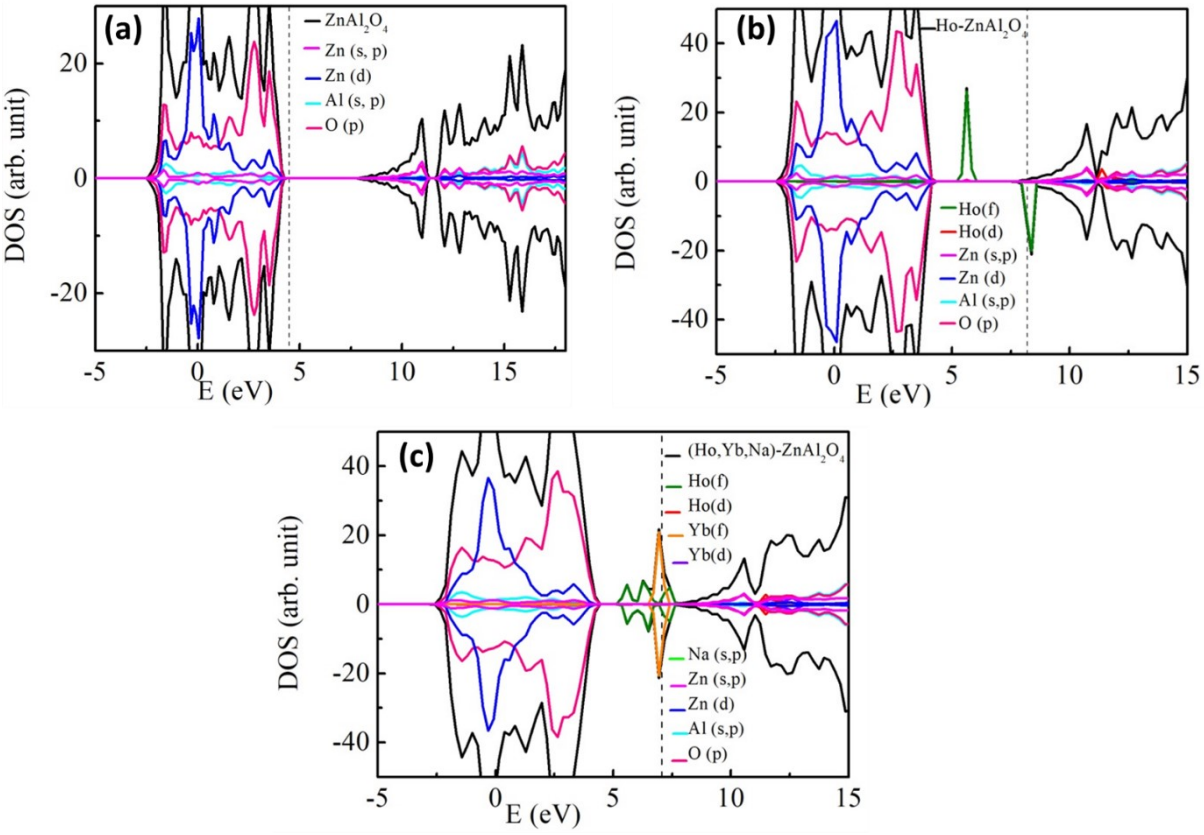

Figure S12: (a) Density of states for $ZnAl_2O_4$, (b) Density of states for Ho-doped $ZnAl_2O_4$ and (c) Density of states for (Ho, Yb, Na)-doped $ZnAl_2O_4$ (Vertical dashed line indicates the Fermi level).

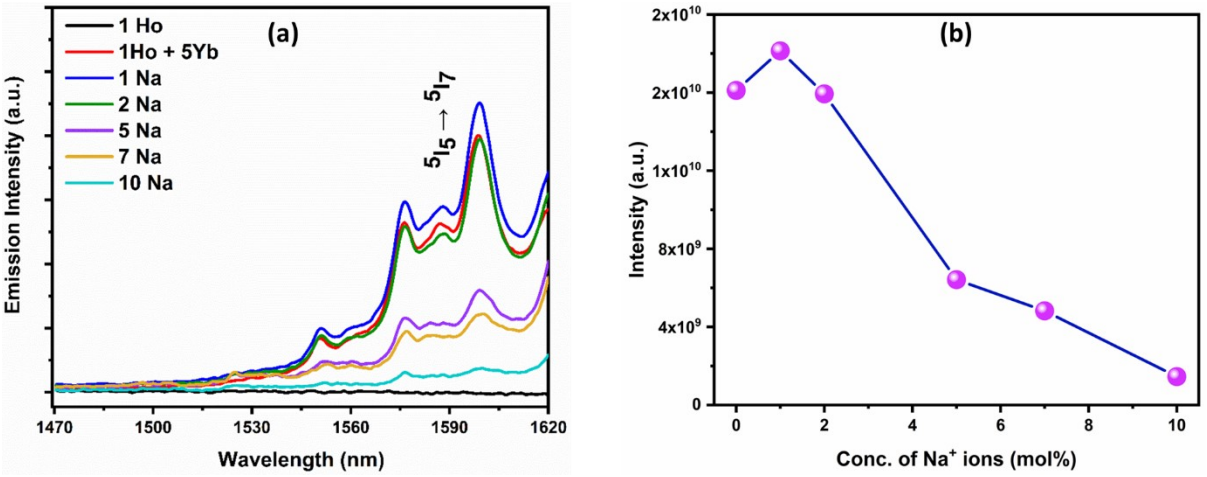

Figure S13: (a) NIR DC emission spectra of doped $ZnAl_2O_4$:1%Ho^{3+}, and codoped $ZnAl_2O_4$:1%Ho^{3+}, 5%Yb^{3+}, *x*%Na^+ (*x* = 0, 1, 2, 5, 7 and 10 mol%) samples under a 980 nm laser excitation at a power of 1.32 W and (b) Variation in DC emission intensities with different concentrations of Na^+ ions.

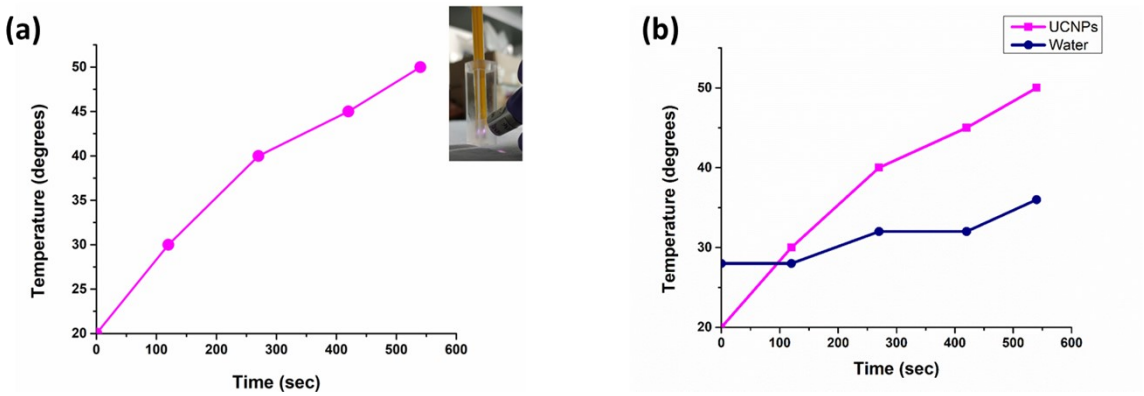

Figure S14: (a) Time-dependent increment in the temperature of $ZnAl_2O_4$:5%Yb^{3+}, 1% Ho^{3+}, 5%Na^+ under 980 nm NIR laser irradiation and (b) Comparison of temperature elevation in control sample with water and with $ZnAl_2O_4$:5%Yb^{3+}, 1% Ho^{3+}, 5%Na^+ sample under 980 nm NIR laser irradiation.

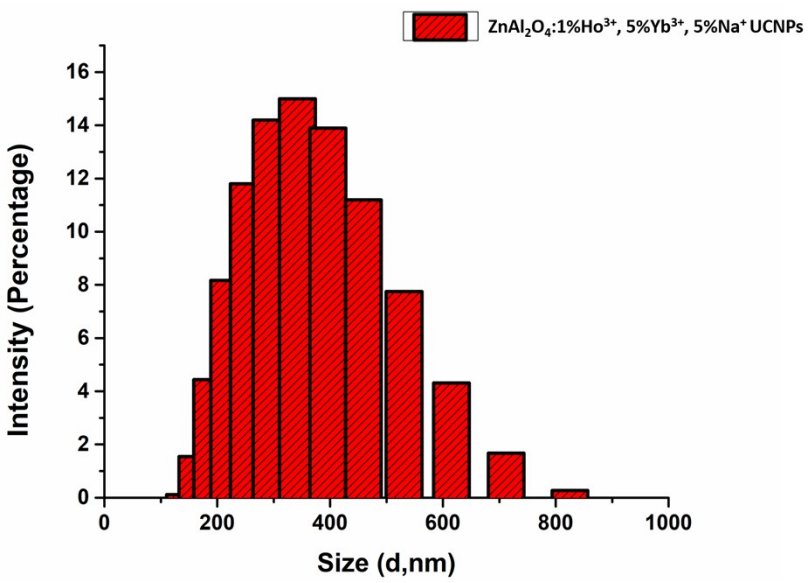

Figure S15: DLS data depicting size distribution profile of the UCNPs.

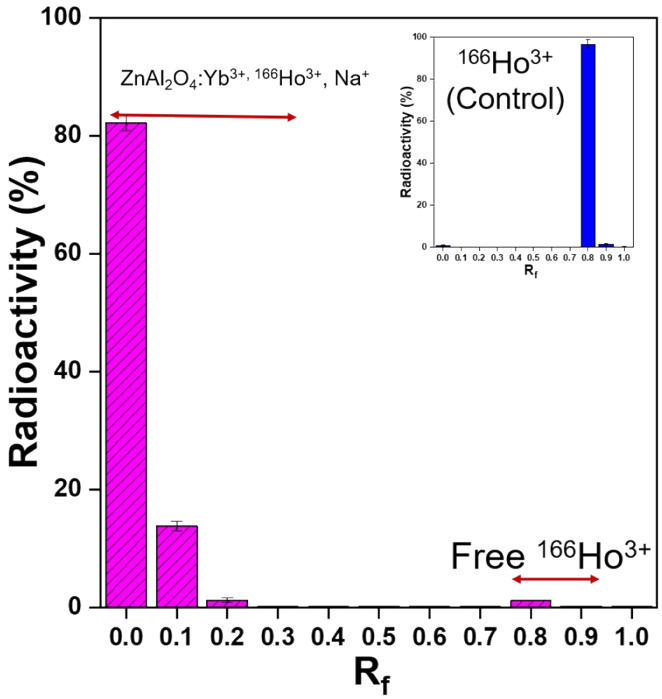

Figure S16: Radio-TLC pattern of $ZnAl_2O_4$:$^{166}Ho^{3+}$,5%Ho^{3+}, 5%Na^+ when developed in citrate buffer. The inset shows the radio-TLC pattern of $^{166}Ho^{3+}$ in the same medium as control.

References

1. Olsen, J. V.; Kirkegaard, P.; Pedersen, N. J.; Eldrup, M., PALSfit: A new program for the evaluation of positron lifetime spectra. *Physica status solidi C* **2007,** 4, (10), 4004-4006.
2. Blöchl, P. E., Projector augmented-wave method. *Physical review b* **1994,** 50, (24), 17953.
3. Kresse, G.; Joubert, D., From ultrasoft pseudopotentials to the projector augmented-wave method. *Physical review b* **1999,** 59, (3), 1758.
4. Perdew, J. P.; Burke, K.; Ernzerhof, M., Generalized gradient approximation made simple. *Physical review letters* **1996,** 77, (18), 3865.
5. Perdew, J. P.; Chevary, J. A.; Vosko, S. H.; Jackson, K. A.; Pederson, M. R.; Singh, D. J.; Fiolhais, C., Atoms, molecules, solids, and surfaces: Applications of the generalized gradient approximation for exchange and correlation. *Physical review b* **1992,** 46, (11), 6671.
6. Monkhorst, H. J.; Pack, J. D., Special points for Brillouin-zone integrations. *Physical review b* **1976,** 13, (12), 5188.
7. Momma, K.; Izumi, F., VESTA: a three-dimensional visualization system for electronic and structural analysis. *Journal of Applied crystallography* **2008,** 41, (3), 653-658.
8. Chakravarty, R.; Guleria, A.; Jadhav, S.; Kumar, C.; Debnath, A. K.; Sarma, H. D.; Chakraborty, S., Bioinspired Synthesis of Intrinsically ^{177}Lu-Labeled Hybrid Nanoparticles for Potential Cancer Therapy. *Industrial & Engineering Chemistry Research* **2020,** 59, (52), 22492-22500.
9. Modak, B.; Ghosh, S. K., Insight into the enhanced photocatalytic activity of $SrTiO_3$ in the presence of a (Ni, V/Nb/Ta/Sb) pair. *Physical Chemistry Chemical Physics* **2018,** 20, (30), 20078-20087.
10. Modak, P.; Modak, B., Exploring the role of vacancy defects in the optical properties of $LiMgPO_4$. *Physical Chemistry Chemical Physics* **2020,** 22, (28), 16244-16257.
11. Vishwakarma, P. K.; Bahadur, A.; Maurya, A.; Rai, S. B., Large enhancement in upconverted green emission intensity from Ho^{3+}/Yb^{3+} co-doped $Y_2Ti_2O_7$ phosphor in the presence of Zn^{2+}. *Materials Research Bulletin* **2019,** 115, 219-226.
12. Perala, R. S.; Singh, B. P.; Putta, V. N. K.; Acharya, R.; Ningthoujam, R. S., Enrichment of Crystal Field Modification via Incorporation of Alkali K^+ Ions in YVO_4:Ho^{3+}/Yb^{3+} Nanophosphor and Its Hybrid with Superparamagnetic Iron Oxide Nanoparticles for Optical, Advanced Anticounterfeiting, Uranyl Detection, and Hyperthermia Applications. *ACS Omega* **2021,** 6, (30), 19517-19528.
13. Yadav, R. S.; Rai, A.; Rai, S. B., NIR light guided enhanced photoluminescence and temperature sensing in $Ho^{3+}/Yb^{3+}/Bi^{3+}$ co-doped $ZnGa_2O_4$ phosphor. *Scientific Reports* **2021,** 11, (1), 1-17.
14. Monika; Yadav, R. S.; Bahadur, A.; Rai, S. B., Near-infrared light excited highly pure green upconversion photoluminescence and intrinsic optical bistability sensing in a Ho^{3+}/Yb^{3+} co-doped $ZnGa_2O_4$ phosphor through Li^+ doping. *The Journal of Physical Chemistry C* **2020,** 124, (18), 10117-10128.
15. Maurya, A.; Yadav, R. S.; Yadav, R. V.; Rai, S. B.; Bahadur, A., Enhanced green upconversion photoluminescence from Ho^{3+}/Yb^{3+} co-doped $CaZrO_3$ phosphor via Mg^{2+} doping. *RSC Advances* **2016,** 6, (114), 113469-113477.
16. Singh, P.; Shahi, P. K.; Rai, A.; Bahadur, A.; Rai, S. B., Effect of Li^+ ion sensitization and optical temperature sensing in Gd_2O_3:Ho^{3+}/Yb^{3+}. *Optical Materials* **2016,** 58, 432-438.
17. Yadav, R. V.; Singh, A. K.; Bahadur, A.; Yadav, T. P.; Yadav, R. S.; Rai, S. B., Effect of Li^+ on frequency upconversion and intrinsic optical bistability of Ho^{3+}/Yb^{3+} co-doped gadolinium tungstate phosphor. *Journal of Physics and Chemistry of Solids* **2018,** 119, 138-146.
18. Krishnan, R.; Menon, S. G.; Poelman, D.; Kroon, R. E.; Swart, H. C., Power-dependent upconversion luminescence properties of self-sensitized Er_2 WO_6 phosphor. *Dalton Transactions* **2021,** 50, (1), 229-239.
19. Sinha, S.; Mahata, M. K.; Swart, H.; Kumar, A.; Kumar, K., Enhancement of upconversion, temperature sensing and cathodoluminescence in the K^+/Na^+ compensated $CaMoO_4$:Er^{3+}/Yb^{3+} nanophosphor. *New Journal of Chemistry* **2017,** 41, (13), 5362-5372.

20. Mi, C.; Wu, J.; Yang, Y.; Han, B.; Wei, J., Efficient upconversion luminescence from $Ba_5Gd_8Zn_4O_{21}$:Yb^{3+},Er^{3+} based on a demonstrated cross-relaxation process. *Scientific Reports* **2016,** 6, (1), 22545.